

Phagocytosis underpins the biotrophic lifestyle of intracellular parasites in the class Phytomyxea (Rhizaria)

Andrea Garvetto¹ , Pedro Murúa² , Martin Kirchmair¹, Willibald Salvenmoser³, Michaela Hittorf¹, Stefan Ciaghi¹, Srilakshmy L. Harikrishnan^{4,5}, Claire M. M. Gachon^{6,7} , John A. Burns⁸  and Sigrid Neuhauser¹ 

¹Institute of Microbiology, University of Innsbruck, Technikerstraße 25, Innsbruck 6020, Tyrol, Austria; ²Laboratorio de Macroalgas, Instituto de Acuicultura, Universidad Austral de Chile, Puerto Montt 5480000, Chile; ³Institute of Zoology, University of Innsbruck, Technikerstraße 25, Innsbruck 6020, Tyrol, Austria; ⁴Centre for Plant Systems Biology, VIB, Zwijnaarde 71, Ghent 9052, Belgium; ⁵Department of Plant Biotechnology and Bioinformatics, Ghent University, Zwijnaarde 71, Ghent 9052, Belgium; ⁶Muséum National d'Histoire Naturelle, UMR 7245, CNRS CP 26, 57 rue Cuvier, 75005 Paris, France; ⁷Scottish Association for Marine Science, Scottish Marine Institute, Dunbeg, Oban, PA37 1QA, UK; ⁸Bigelow Laboratory for Ocean Sciences, 60 Bigelow Dr., East Boothbay, ME 04544, USA

Summary

Author for correspondence:
Sigrid Neuhauser
Email: sigrid.neuhauser@uibk.ac.at

Received: 9 September 2022
Accepted: 6 February 2023

New Phytologist (2023) **238**: 2130–2143
doi: 10.1111/nph.18828

Key words: algal pathogen, Brassicaceae, *Ectocarpus siliculosus*, *Maullinia ectocarpii*, phagotrophy, plant pathogen, *Plasmodiophora brassicae*, trophic mode.

- Phytomyxea are intracellular biotrophic parasites infecting plants and stramenopiles, including the agriculturally impactful *Plasmodiophora brassicae* and the brown seaweed pathogen *Maullinia ectocarpii*. They belong to the clade Rhizaria, where phagotrophy is the main mode of nutrition. Phagocytosis is a complex trait of eukaryotes, well documented for free-living unicellular eukaryotes and specific cellular types of animals. Data on phagocytosis in intracellular, biotrophic parasites are scant. Phagocytosis, where parts of the host cell are consumed at once, is seemingly at odds with intracellular biotrophy.
- Here we provide evidence that phagotrophy is part of the nutritional strategy of Phytomyxea, using morphological and genetic data (including a novel transcriptome of *M. ectocarpii*). We document intracellular phagocytosis in *P. brassicae* and *M. ectocarpii* by transmission electron microscopy and fluorescent *in situ* hybridization.
- Our investigations confirm molecular signatures of phagocytosis in Phytomyxea and hint at a small specialized subset of genes used for intracellular phagocytosis. Microscopic evidence confirms the existence of intracellular phagocytosis, which in Phytomyxea targets primarily host organelles.
- Phagocytosis seems to coexist with the manipulation of host physiology typical of biotrophic interactions. Our findings resolve long debated questions on the feeding behaviour of Phytomyxea, suggesting an unrecognized role for phagocytosis in biotrophic interactions.

Introduction

Often seen as a conserved and nearly universal trait, present in nearly all major eukaryote lineages, phagocytosis underpins defining eukaryotic features such as the origin of endosymbiotic organelles and of the endomembrane system (Raven *et al.*, 2009; Yutin *et al.*, 2009). Phagocytosis is defined as the interiorization and internal digestion of particles larger than 0.5 μm (Flannagan *et al.*, 2012) and it is assumed to be the principal mode of nutrition in the majority of free-living heterotrophic microbial eukaryotes (thereby called phagotrophy). Other heterotrophic microbial eukaryotes feed by osmotrophy (i.e. the extracellular digestion and/or absorption of molecules via the cell membrane) or pinocytosis (i.e. the engulfment of solubilized particles by membrane invaginations), both of which are common in intracellular parasites, though not exclusive to them (Seenivasan *et al.*, 2013; Spielmann *et al.*, 2020).

Despite its pervasiveness among eukaryotes, we owe most of the information on phagocytosis to a special group of ‘professional phagocytes’ from the immune system of vertebrate model organisms (Uribe-Querol & Rosales, 2020), for which molecular tools and laboratory experiments are possible. The investigation of phagotrophy and other trophic modes can be challenging in microbial eukaryotes and it relies heavily on microscopic observations and on the labelling/tracking of food items (Keymer *et al.*, 2017; Miura *et al.*, 2017; Godrijan *et al.*, 2022). Even extensive observational evidence may alone be insufficient in establishing the feeding strategy of an organism (Not *et al.*, 2007; Moreira & Lopez-Garcia, 2014). Phagotrophy is used as an example of a range of ‘nearly behavioural’ traits of microbial eukaryotes, the study of which requires a combination of molecular and laboratory-based investigations (Keeling, 2019).

Intracellular eukaryotic parasites can obtain macromolecules from their host via endocytosis, that is phagocytosis of solid food

particles and pinocytosis of fluids and the solutes therein. For example, Apicomplexa such as *Plasmodium* spp. (Abu Bakar *et al.*, 2010; Matz *et al.*, 2020) and *Toxoplasma gondii* (Dou *et al.*, 2014) ingest and digest macromolecules and pieces of host cell cytoplasm via endocytosis. The kinetoplastid, *Trypanosoma cruzii*, has been reported to phagocytotically take up nutrients via the cytostome, a well-defined tubular structure conserved from its free-living ancestors (Chasen *et al.*, 2020). Some intracellular parasites of fungi, oomycetes and green algae (*Rozella polyphagi* and *Rozella allomycis*; Fungi, Cryptomycota) have been observed to actively engulf host cytoplasm and organelles, but also to recruit host mitochondria around their thallus, seemingly compensating for their own unstructured and depauperated ones (James *et al.*, 2013; Powell *et al.*, 2017). These findings place *Rozella* (together with the earlier-cited intracellular parasites of animals) in a particular trophic niche where conserved traits from free-living ancestors (e.g. phagotrophy) and derived traits co-evolved with the host (e.g. host manipulation) coexist within the same biotrophic organism.

With the notable exception of the photosynthetic chlorarachnids, phagotrophy is assumed to be the main mode of nutrition in almost all the free-living Rhizarians (Cavalier-Smith *et al.*, 2018). Within this clade, Phytomyxea are a class of unicellular eukaryotic parasites living as intracellular obligate biotrophs in plants and stramenopiles in marine, freshwater and terrestrial habitats (Bulman & Neuhauser, 2017; Cavalier-Smith *et al.*, 2018). The class is currently split into three main clades: the orders Plasmodiophorida and Phagomyxida (Hittorf *et al.*, 2020) and the recently described genus *Marinomyxa* (Kolátková *et al.*, 2020). Phylogenetically, Phytomyxea are sister to the free-living Vampyrellida (Sierra *et al.*, 2016; Cavalier-Smith *et al.*, 2018) and Aquavolonida (Bass *et al.*, 2018). Aquavolonida are a group of small, unicellular, free-living phagotrophic flagellates (Bass *et al.*, 2018). Vampyrellida are amoebae with different modes of prey item consumption, ranging from classic phagocytic predation to specialized protoplast feeding; in which the target cell wall is perforated and the amoeba infiltrates the space between the wall and the plasma membrane to phagocytize its prey (Hess & Suthaus, 2022). Phytomyxea use a different strategy to achieve a similar result, piercing the cell wall with a sophisticated extrusome called Rohr and Stachel (Keskin & Fuchs, 1969; Aist & Williams, 1971) to gain access to the host cytoplasm (Williams & McNabola, 1970; Maier *et al.*, 2000); although clear evidence on how exactly phytomyxids cross the host plasma membrane is still missing. Phytomyxea reach the host cell as flagellated zoospores and penetrate into it as small unicellular protoplasts, later developing into larger intracellular multinucleate feeding plasmodia. Plasmodia can be of two types: short-lived (*c.* 7 d) sporangial plasmodia, developing into clusters of sporangia (i.e. sporangiosori) and directly releasing infective flagellated zoospores; or sporogenic plasmodia actively growing as biotrophs inside the living host cell (*c.* 3–4 wk) before developing thick-walled overwintering resting spores (i.e. sporosori). During that time, sporogenic plasmodia induce hypertrophy of the infected cells which, coupled with induced hyperplasia of the tissue, leads to the formation of galls in the host (Murúa *et al.*, 2017; Olszak

et al., 2019). Manipulation of Brassicaceae hosts by *Plasmodiophora brassicae* induces hypertrophied infected cells to act as physiological sinks, driving photosynthates from the aerial parts of the plant (Malinowski *et al.*, 2019) and inducing their accumulation as starch grains in the root (Ma *et al.*, 2022).

How Phytomyxea feed on their host has never been clearly elucidated and even the trophic mode of the model phytomyxean *P. brassicae* is still debated (Bulman & Neuhauser, 2017). Among the Phagomyxida, the brown seaweed parasite *Phagomyxa algarum* and the diatom parasites *Phagomyxa odontellae* and *Phagomyxa bellerocheae* have been observed to ingest the cytoplasm and organelles from their hosts by phagocytosis and accumulate the digested material in pigmented digestive vacuoles (Karling, 1944; Schnepf, 1994; Schnepf *et al.*, 2000). On the other hand, the lack of a conspicuous digestive vacuole and failure to detect engulfed host organelles has led to the conclusion that another brown seaweed-infecting phagomyxid *Maullinia ectocarpii* feeds by osmotrophy (Maier *et al.*, 2000). Within the Plasmodiophorida, intracellular phagotrophy has been observed in the oomycete-infecting species *Woronina pythii* (Dylewski *et al.*, 1978) and *Octomyxa brevilegniae* (Couch *et al.*, 1939; Pendergrass, 1950). Food vacuoles containing residues of cytoplasm and organelles from the host plant *Nasturtium officinale* (watercress) have also been found in *Hillenburgia nasturtii* (formerly *Spongospora subterranea* f. sp. *nasturtii*; Clay & Walsh, 1997; Hittorf *et al.*, 2020). Despite sparse electron microscopy evidence supporting the existence of phagotrophy in *P. brassicae* (Williams & McNabola, 1967; Buczacki, 1983), a clear consensus on whether nutrition is dominated by osmotrophy, phagotrophy or consists of a mix of the two has not yet been reached (Dylewski, 1990).

Molecularly, complex and 'behavioural' traits such as feeding modes are inherently difficult to investigate, since they are the final phenotypic outcome of a cohort of finely tuned genes involved in a range of overlapping (and often widely conserved) biological processes (Keeling, 2019). *In silico* predictions based on the presence or absence of genome-wide molecular signatures identified in organisms known to possess a certain phenotypic trait can be used to infer the likelihood of the existence of that specific trait in other organisms, based on their genomic information (Burns *et al.*, 2018). Direct observation, laboratory-based experiments and analysis of molecular data are complementary and have been successfully used to identify or rule-out phagotrophy in different groups of prasinophyte green algae (Bock *et al.*, 2021; Jimenez *et al.*, 2021).

In this study, we used genomic and transcriptomic data from the plasmodiophorids *P. brassicae* and *S. subterranea* (Schwelm *et al.*, 2015; Rolfe *et al.*, 2016; Ciaghi *et al.*, 2018, 2019); and sequenced the transcriptome of the infective stage of the phagomyxid *M. ectocarpii* to detect molecular signatures of phagotrophic behaviour (i.e. protein families present in well-known phagocytes) in the class Phytomyxea. We complemented results from these analyses with fluorescent and electron microscopy observations, to investigate whether: intracellular plasmodia engulf organelles and parts of the host cell; the molecular machinery underpinning the phagocytic behaviour is present; and intracellular plasmodia express core genes involved in

phagocytosis, similarly to other intracellular phagocytes (e.g. *R. allomyces*).

Materials and Methods

Maullinia ectocarpii transcriptome: biological material, RNA extraction, sequencing and data processing

The model brown alga *Ectocarpus siliculosus* (Dillwyn) Lyngbye, 1819 strain Ec32m (CCAP 1310/4) was used as a host for the cocultivation of *M. ectocarpii* Maier, E. R. Parodi, R. Westermeier et D. G. Müller 2000 (CCAP 1538/1) for RNA extractions. The pathosystem was maintained in half strength Provasoli medium at 15°C, with a 12 h : 12 h photoperiod, and an irradiance of 10 $\mu\text{mol m}^{-2} \text{s}^{-1}$. Quadruplicates of *E. siliculosus* Ec32m infected with *M. ectocarpii* were generated, harvested after 21 d with a 70 μm cell strainer (VWR, Radnor, PA, USA), and transferred immediately to ice-cold RNeasy lysis buffer (Ambion, Austin, TX, USA), stored overnight at 4°C, and transferred at -80°C until used for RNA extraction. Samples in RNeasy lysis buffer were thawed on ice, vortexed and briefly spun down. Five hundred microlitre was transferred onto a pre-mixed Bead-matrix (D1034-MX; Biozym, Hessisch Oldendorf, Germany). Samples were then spun down at 10 000 g, 4°C for 10 min, and RNeasy lysis buffer was carefully removed. Samples were immediately snap frozen in liquid nitrogen. Frozen material was subsequently homogenized with a FastPrep (MP Biomedicals, Santa Ana, CA, USA) for 40 s at 6 m s⁻¹. This step was repeated three times and samples were returned into liquid nitrogen in between the three cycles to aid homogenization and avoid RNA degradation. After the last homogenization round, samples were transferred into liquid nitrogen and placed on ice. Four hundred and fifty microlitre buffer RLT (+ β -mercaptoethanol) from the Qiagen RNeasy Plant Mini Kit (Qiagen) were added, samples were vortexed for 30 s and spun down briefly before processing them according to the manufacturer's instructions with an additional ethanol (95%) washing step before RNA elution. RNA quality was tested on an Agilent Bioanalyzer 2100 (Agilent Technologies, Palo Alto, CA, USA). Poly-A selected strand-specific library construction and paired-end sequencing (2 \times 125 bp on a HiSeq 2500 using v.4 chemistry; Illumina, San Diego, CA, USA) was performed at the VBCF NGS Unit (Vienna, Austria). Quality of the raw reads was checked using FASTQC v.0.9.1 (Andrews, 2010). Illumina adapters were removed and only good quality reads (sliding window 5 bp; average quality score > 20) with a minimum length of 50 bp were kept using TRIMMOMATIC v.0.36 (Bolger *et al.*, 2014). Bacterial contamination was removed from the remaining reads using DECON-SEQ v.0.4.3 (Schmieder & Edwards, 2011). Reads from the mock and infected samples were separately mapped against the Ec32m reference genome v.2 (Cock *et al.*, 2010) using BOWTIE2 v.2.2.4 (Langmead & Salzberg, 2012). Unmapped reads from the mock samples were *de novo* assembled into transcripts using TRINITY v.2.4.0 (Grabherr *et al.*, 2011) with default settings for k-mer size (25 bp) and minimum contig length (200 bp). These transcripts were further used as a reference to filter out host reads from the infected samples and select only reads unambiguously assigned to *M. ectocarpii* (i.e. unmapped reads of this filtering step). Remaining

reads were *de novo* assembled into transcripts using TRINITY with default settings, thus constituting *M. ectocarpii* transcriptome. Read counts (i.e. gene expression) of the assembled transcripts was estimated using RSEM (Li & Dewey, 2011) included in the TRINITY suite. Only transcripts with FPKM (fragments per kilobase per million reads) values > 1 were kept for downstream analysis. Completeness of the transcriptome was verified using BUSCO v.5.2.2 running in transcriptome mode with the eukaryote_odb10.2019-11-20 reference gene set (Simão *et al.*, 2015). An inferred *Maullinia* proteome was generated using the longest open reading frames and the protein coding genes predicted by TRANSDCODER v.5.0.2 (<https://github.com/TransDecoder>) with default settings and used in downstream analyses. Functional annotation of the predicted genes was achieved using INTERPROSCAN v.5 (Jones *et al.*, 2014).

Additional molecular data

Transcriptome data from an Austrian population of *P. brassicae* Woronin, 1877 were taken from Ciaghi *et al.* (2018). Publicly available genomic data were taken from *P. brassicae* strains e3 (Schwelm *et al.*, 2015) and PT3 (Rolfe *et al.*, 2016); and *S. subterranea* (Wallr.) Lagerh. 1892 strain K13 (Ciaghi *et al.*, 2018).

In silico predictions of trophic mode

BUSCO v.5.2.2 was run in proteome mode against the eukaryote_odb10.2019-11-20 reference gene set (Simão *et al.*, 2015) to assess completeness of all inferred proteomes, allowing for accurate predictions of trophic modes (Liu *et al.*, 2021). Genomic and transcriptomic data from all three species of phyto-myxean parasites in this study show a high degree of BUSCO completeness (< 105 missing BUSCOs over the total 255 BUSCOs in the eukaryota_odb10 database), indicating that their trophic mode can be accurately assigned by TROPICMODEPREDICTIONTOOL. In particular, complete and fragmented BUSCOs amounted to: 215 for *M. ectocarpii*, 236 for *P. brassicae* e3, 233 for *P. brassicae* PT3, 194 for *P. brassicae* transcriptome and 224 for *S. subterranea* (Supporting Information Fig. S1).

The TROPICMODEPREDICTIONTOOL tool (Burns *et al.*, 2018) was used to predict the trophic mode of the investigated organisms *in silico*, based on the molecular signatures for phagotrophy, photosynthesis and prototrophy (i.e. organisms capable of synthesizing arginine, lysine, threonine, biotin, vitamin B₁, B₂ and B₆; here used as a proxy for osmotrophic feeding). The code (available at <https://github.com/burnsajohn/predictTrophicMode>) was run in the default mode. Prediction scores enumerate the probability that an organism has the genetic toolbox to carry out the indicated function on a scale of 0–1.

Besides the three main trophic modes listed earlier, special forms of phagocytosis evolved to target a specific range of substrates, such as that of the extracellular parasite *Entamoeba histolytica* (feeding on apoptotic vertebrate cells and erythrocytes) and of the intracellular parasite *R. allomyces* (feeding on fungal cytoplasm and organelles) are predicted via an emended subset of molecular signatures of phagocytosis. Predictions were visualized as bar charts and by projecting the 4-dimensional probability values onto a 3D

tetrahedral shape representing the three trophic modes (or their absence) using scripts modified from the R package 'PAVO' (Doucet *et al.*, 2013). For static visualization of the trophic mode of an organism, the 3D tetrahedral shape with the summary prediction from each organism plotted onto it is finally rendered as a 2D circular Mollweide projection as described in Bock *et al.* (2021) and Jimenez *et al.* (2021). A detailed overview of the genes best matching the predictive molecular signatures is presented in Notes S1 for the comparison between *P. brassicae* e3 genome and *P. brassicae* transcriptome; as well as for the comparison between *P. brassicae* transcriptome and *M. ectocarpii* transcriptome.

Fluorescent *in situ* hybridization and optical microscopy

Plasmodiophora brassicae was grown on the host plant *Brassica rapa* L. var. *pekinensis* (cv 'Granat') for 61 d before collection of root galls, thus allowing for the presence of a high number of plasmodia at different stages of development. Plants were grown at 20°C with a 12 h : 12 h photoperiod and an average irradiance of 135 $\mu\text{mol m}^{-2} \text{s}^{-1}$. Galls were thoroughly rinsed in tap water to remove soil residues and preserved in Histofix 4% (phosphate-buffered formaldehyde solution; Carl Roth, Karlsruhe, Germany) for *c.* 1 h. Following fixation, galls were dehydrated in ascending ethanol series: 10 min in 50% ethanol, twice 10 min in 70% ethanol and final storage in absolute ethanol. Galls were prepared for fluorescence *in situ* hybridisation (FISH) staining following the procedure detailed in Schwelm *et al.* (2016), with a few modifications. Briefly, galls were hand-cut into thin sections and rinsed for 10 min in hybridization buffer (900 mM NaCl, 20 mM Tris-HCl pH 7.5, 35% formamide, 0.01% SDS) before incubation overnight at 46°C in the dark in hybridization buffer, amended with 50 ng of the FISH probe PI_LSU_2313 (Table 1). Samples were washed twice for 20 min in washing buffer (900 mM NaCl, 20 mM Tris-HCl pH 7.5, 5 mM of NaEDTA pH 8, 0.01% SDS) at 48°C. Samples were then incubated for 20 min in Hoechst 33342 (Thermo Scientific, Waltham, ME, USA) diluted 1000 \times in distilled water, before being mounted in Vectashield (H-1000; Vector Laboratories, Burlingame, CA, USA). *Maullinia ectocarpii* was grown on *E. siliculosus* Ec32m male gametophyte or *Macrocystis pyrifera* (L.) C. Agardh, 1820 CCAP1323/1 female gametophyte (same culture conditions specified earlier) for 1 month before collection. Fixation and FISH staining were achieved in the same way described for *P. brassicae*, with the following adjustments. After fixation in 4% Histofix infected algae were incubated for 2 min in 30% H_2O_2 to increase cell wall permeability and then dehydrated in ascending ethanol series. The hybridization was performed at 46°C overnight in the dark in hybridization buffer amended with 50 ng of probe MauJ17 (Table 1). Slides were observed with a Nikon Eclipse Ti2-E microscope (Nikon, Tokyo, Japan) equipped

with an Andor Zyla 5.5sCMOS monochrome camera (Andor Technology, Belfast, UK) and Nikon CFI Plan-Fluor $\times 40/0.75$ NA and $\times 60/0.85$ NA objectives. The excitation wavelength for Hoechst 33342 was 365 nm, whereas it was 490 nm for FISH probes (Table 1). The NIS ELEMENTS software (Nikon) was used for image analysis and post-processing (generation of overlaid images, z-stack analysis and export of z-stack as videos). Final figures were composed using INKSCAPE 0.92.4 (Inkscape Project, New York, NY, USA).

Transmission electron microscopy

For transmission electron microscopy (TEM), *M. ectocarpii* was grown on healthy female gametophytes of *M. pyrifera* CCAP 1323/1 in $\frac{1}{2}$ strength Provasoli medium, at 10°C, under 2–6 $\mu\text{mol m}^{-2} \text{s}^{-1}$ white light irradiation and 12 h : 12 h photoperiod. Biological material was chemically fixed and processed as per Murúa *et al.* (2017). Briefly, the biomass was immersed in a solution composed of 2.5% glutaraldehyde, 0.1 M cacodylate buffer at pH 7.4, 0.5% caffeine, 0.1% CaCl_2 and 0.3% NaCl in Provasoli-enriched seawater for 2–3 d. Post-fixation staining was achieved with 1% OsO_4 and 2% uranyl acetate. After dehydration in acetone series, samples were embedded in Spurr resin and polymerized at 60–70°C. Blocks were cut into 90 nm-thick sections using an UC6 ultramicrotome (Leica, Wetzlar, Germany) mounted on copper grids and counterstained with lead citrate. Imaging was achieved with a JEM-1400 Plus (Jeol, Akishima, Tokyo, Japan) TEM with an AMT UltraVue camera (Woburn, MA, USA). For TEM imaging of *P. brassicae*, root galls of *B. rapa* var. *pekinensis* were collected from field material in Weer (Tirol, Austria) in September 2018. Specimens were chemically fixed with 2.5% glutaraldehyde in 0.1 M cacodylate buffer containing 10% sucrose for 1 h at 4°C, rinsed with cacodylate buffer and post fixed with 1% osmium tetroxide in 0.05 M cacodylate buffer for 1 h at 4°C. After washing in cacodylate buffer, samples were dehydrated with an increasing acetone series and embedded in EMBED 812 resin. Ninety nanometre-thick cross-sections of root galls were cut with an Ultracut UCT (Leica), mounted on grids and counterstained with lead citrate. Sections were examined with a Libra 120 energy filter TEM (Zeiss) and images were taken with a TRS 2 \times 2k high speed camera (Tröndle, Munich, Germany) and an IMAGESP software (Tröndle).

Results

In silico prediction of trophic modes of Phytomyxea using genomic and transcriptomic signatures

All analysed phytomyxids datasets bear molecular signatures of phagotrophy (Fig. 1; Table S1). *Plasmodiophora brassicae* (e3 and

Table 1 Fluorescent *in situ* hybridization probes used in this study.

Probe	Organism/gene	Sequence	Dye	Excitation λ (nm)
PI_LSU_2313	<i>Plasmodiophora brassicae</i> /28S rRNA	CCAGGCCTTTCAGCCAAGTA	6-FAM	490
MauJ17	<i>Maullinia ectocarpii</i> /18S rRNA	CACGTCCCTCGTACCCGT	6-FAM	490

Phagocytosis, prototrophy, and photosynthesis predictions

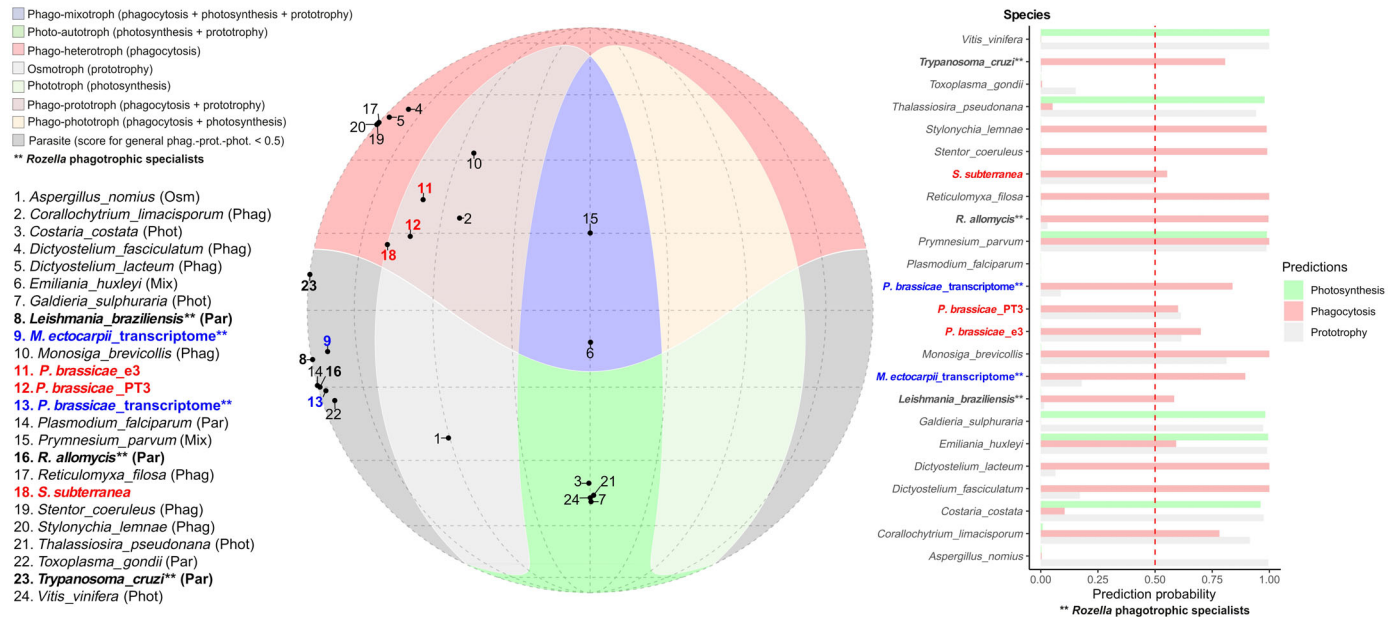


Fig. 1 Mollweide projection showing the position of predicted phagotrophs, prototrophs and photosynthetic organisms; and bar chart showing the scores of individual prediction probabilities for the same organisms. Colored regions (red, blue, beige, green) indicate overlapping areas where individual predictions were > 0.50 . Dark-grey shaded regions indicate areas where all three predictions were < 0.50 . Note that phagotrophic specialists (such as *Rozella*-like phagotrophs) do not map the three main trophic categories and fall in the grey area due to the Mollweide projection only using the general phagocytosis prediction for each organism. Each numbered black dot indicates one of the 19 organisms used as a reference to test the model. The same organisms are represented in the bar chart where prediction probability scores are shown as coloured bars (green, photosynthetic; grey, prototroph; brown, phagotroph). The 0.5 threshold, above which a prediction is deemed valid, is indicated by the red dashed line. Names in red/bold indicate the phytomyxid genomes tested in this study while blue/bold indicates phytomyxid transcriptomes; names in bold and followed by double asterisks (**) indicate organisms for which the strongest prediction is *Rozella*-type intracellular phagotrophy.

PT3) and *S. subterranea* (SSUBK13) genomes score high for phago-prototrophy (red nos. 11, 12 and 18 on the Mollweide projection in Fig. 1). The prediction scores from the genome data in *P. brassicae* are *c.* 60% for prototrophy ($e3 = 0.615$ and PT3 = 0.612) and are similar for general phagotrophy ($e3 = 0.700$; PT3 = 0.600). The prototrophy score for *S. subterranea* is lower (SSUBK13 = 0.500, bar chart in Fig. 1), as is the score for general phagotrophy (SSUBK13 = 0.552). When the subset of signatures predicting *Rozella*-like intracellular phagotrophy is considered the probability scores increase to nearly 100% for the genome datasets ($e3 = 0.978$; PT3 = 0.983 and SSUBK13 = 0.967; bar chart in Fig. 1). The probabilities for photosynthesis and entamoebid-like phagotrophy (a second peculiar mode of phagotrophy mostly observed in extracellular endoparasites such as *Entamoeba*) remain below the threshold of 50% in the genomic data (Table S1). When the proteomes inferred from the transcriptomes of *P. brassicae* and *M. ectocarpii* are tested the score for general phagotrophy and prototrophic predictions are very low (< 0.21). The *Rozella*-like phagotrophy remains high with a score of 0.838 in *P. brassicae* and 0.894 in *M. ectocarpii* (bar chart in Fig. 1). The transcriptome datasets are placed in the section 'Parasite' of the Mollweide projection and map close to the intracellular fungal parasite *R. allomycis* (red nos. 9 and 13 and black no. 16 in the Mollweide projection in Fig. 1), while the genomic

datasets are in the phago-prototroph area. The assignment to the 'Parasite' area in the Mollweide projection highlights a low score (< 0.5) for the main trophic categories (i.e. general phagotrophy, prototrophy and photosynthesis), but does not exclude the assignment to specialized sub-categories of phagocytosis (i.e. *Entamoeba* or *Rozella*-like phagocytosis) as highlighted by the bar chart in Fig. 1.

In *P. brassicae* (for which both genomic and transcriptomic data are available), a detailed look at the molecular signatures highlighted that nearly half (14/29) of the phagotrophy-related genes driving the genome apart from the transcriptome were associated with cilia/flagella (as per their GO term annotation, Notes S1). Within the predictive model, flagella and cilia are descriptors of the phago-prototrophic niche, which accommodates organisms using these structures to feed (e.g. choanoflagellates such as *Monosiga brevicollis*; Fig. 1).

On the other hand, trophic predictions for the transcriptomic datasets of *P. brassicae* and *M. ectocarpii* were similar (Fig. 1). In *P. brassicae* genes associated with phagotrophic signatures in the transcriptome were linked to GO terms involving the cytoskeleton (14/40), the cytosol (6/40) and the mTOR complexes (5/40), including the GO terms TORC2 complex, Seh1-associated complex and the lysosome gene RRAGA (Notes S1). A closer look at the predicted functions highlights their potential

involvement in processes such as signal transduction, cell reorganization/polarization, metabolism and cell cycle. In particular, Ras GTPases, mTORC1 and mTORC2 complexes are strong descriptors of *Rozella*-like phagotrophic behaviour and describe nearly half (10/21) of the signatures shared between the transcriptomes of *P. brassicae* and *M. ectocarpii* (Notes S1).

Microscopic evidence of phagocytosis in intracellular plasmodia of *P. brassicae* and *M. ectocarpii*

Microscopic observation of intracellular biotrophic plasmodia of *P. brassicae* and *M. ectocarpii* support phagotrophy of host organelles by the parasites. Mature feeding plasmodia of *P. brassicae* (Fig. 2a) could be recognized by the high number of small nuclei (Fig. 2b'–d', small blue dots) in the absence of cytoplasm cleavage. The plant nucleus was still present and could be distinguished from the parasite nuclei by its larger dimensions (Fig. 2b,b'; white triangle). Plasmodia filled up the host cells entirely (Fig. 2a–d; green), leaving little free space within the cell wall. Abundant starch grains were easily identified in differential interference contrast microscopy by their shape, size, hyaline texture and tridimensional appearance (Fig. 2b''–d''). A high number of starch grains was located between the plant cell wall and the parasite plasma membrane, pressed against the plasmodium as if superficially 'plugged' in membrane pockets (Fig. 2b,b',d,d'). Many starch grains were also found to be completely enveloped by the parasite plasmodium, often contiguous to other engulfed and 'plugged' starch grains, giving the plasmodium an overall 'sponge-like' or 'trabecular' aspect in fluorescence microscopy (Fig. 2b'–d'). Two starch grains were entirely surrounded by the plasmodium (Fig. 2c,c',c'', white arrowheads; videos in Notes S2) as highlighted by the presence of green hue around them and in the focal planes above and below them.

Ectocarpus siliculosus cells infected by mature *M. ectocarpii* were easily distinguishable thanks to the clear signs of hypertrophy (Fig. 2e, white square). The plasmodium shown (Fig. 2f–h) occupied the majority of the space within the host cell wall, as indicated by the green FISH staining of its cytoplasm. The plasmodium was multinucleated (Fig. 2f–h,f'–h', blue signal) and showed vacuolar structures where no green fluorescence could be observed (Fig. 2f–h,f'–h', white arrowheads and asterisk; videos in Notes S2). Some vacuoles contained refractive structures consistent with the phaeoplasts of *E. siliculosus* (Fig. 2g,g',g'', white arrowheads) while other did not (Fig. 2g,g',g'', white asterisk). Phaeoplasts were also observed to be 'plugged' in membrane pockets (Fig. 2f,f',f'',h,h',h'', white arrowhead), much like starch grains in *P. brassicae*. Scans of the entire volume of the investigated plasmodia along the *z*-axis are available as videos (Notes S2); allowing for a better visualization of the host organelles engulfed by the parasites. To further strengthen our observations, we performed a FISH experiment on *M. ectocarpii* infecting the female gametophyte of the kelp *M. pyrifera*. Even in this case, phagocytosis was observed as highlighted by the observation of phagocytic vacuoles and the late phagocytosis of the host nucleus (Fig. S2; Notes S3).

Ultrastructural evidence of phagocytosis in intracellular plasmodia of *P. brassicae* and *M. ectocarpii*

Plasmodia and thick-walled resting spores of *P. brassicae* were observed inside the cortical cells of *B. rapa* ssp. *pekinensis*. Plasmodia can be discriminated from the plant host because of the high amount of lipid globules stored within the cytoplasm (absent from healthy plant cortical cells), the different electron opacity of the cytoplasm and the relatively poorly stained mitochondria with sparse tubular cristae (Fig. 3). Multinucleate plasmodia occupy most of the host cell, leaving space only for the host nucleus, small vacuoles and few smaller organelles (like mitochondria) embedded in a film of plant cytoplasm appressed to the cell wall. Parasite nuclei were clearly distinguishable from the plant nuclei, because of their rounder shape and smaller size (Fig. 3a,a'). The overall shape of the plasmodium was irregularly lobed, to the extent that often it was impossible to clarify whether a single highly lobed or many different plasmodia were inhabiting the same host cell (Fig. 3a,a'). Lobes of different shape and size were often found surrounding and/or closely appressed to starch grains (Fig. 3b,b'), originated from desegregated amyloplasts. Often pseudopodia-like processes and membrane invaginations seemed to encircle and close around starch grains (Fig. 3c,c',d,d') and in one occasion one of those granules was found to be completely surrounded by the plasmodium (Fig. 3a, StG). The mitochondria of *P. brassicae* were found to be generally electron-translucent and contained fewer cristae than the lamellar plant mitochondria (Fig. 3c,c',d,d', asterisks). Mitochondria in thick-walled resting spores were much better defined in their ultrastructure and are overall more electron opaque (Fig. S3).

Feeding plasmodia of *M. ectocarpii* were observed in intercalary and tip cells of the filamentous female gametophytes of *M. pyrifera* (Fig. 4). Plasmodia readily occupy the whole host cell, initially taking up the space of the central vacuole, thereby pushing the organelles towards the periphery of the cell. *M. ectocarpii* plasmodia are easily discriminated from the host cell by the absence of phaeoplasts and because of the difference in the cytoplasmic electron opacity (i.e. opaquer in the alga; Fig. 4). Electron dense mitochondria with tubular cristae have been noticed in the algal host. In the plasmodia of *M. ectocarpii*, mitochondria are not as visible: putative mitochondria appear as double-membrane bounded electron translucent structures without clearly discernible tubular cristae (Figs 4a,a',b,b', asterisks, S3). Comparably with observations in *P. brassicae*, in mature *M. ectocarpii* plasmodia/zoosporangia, mitochondria within zoospores show a higher level of structure, being electron-denser and with well-organized tubular cristae (Fig. S3). Plasmodia are irregular and sometimes structures similar to pseudopodia can be observed, especially in very young, developing plasmodia which do not yet fill the host cell (Fig. S4). Vacuoles are often observed within *M. ectocarpii* plasmodia and differ in size and content (Fig. 4a',b', arrows and nos. 1–3). Vacuoles can be nearly empty (electron translucent), but most vacuoles are either loosely filled with degraded material (Fig. 4a',b', no. 2) or filled with host organelles and cytoplasm (Fig. 4a',b', nos. 1 and 3). In Fig. 4(b,b') vacuole no. 3 can be observed containing a phaeoplast, with

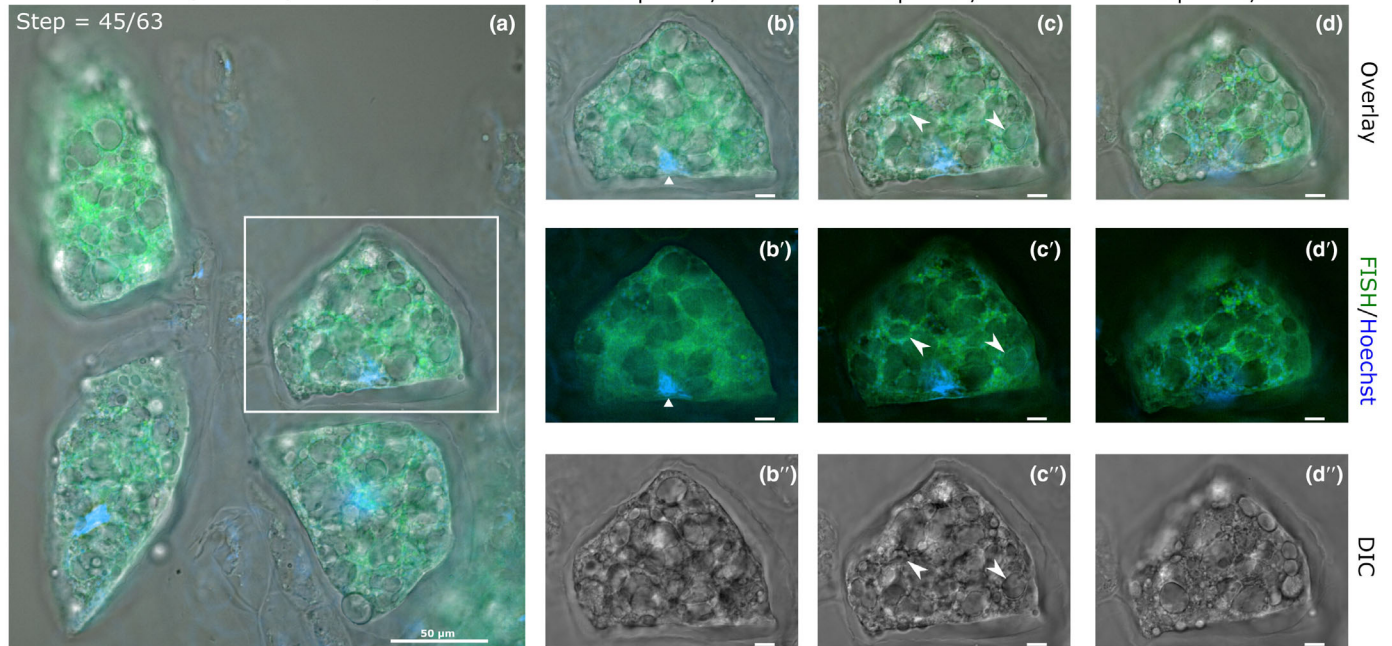
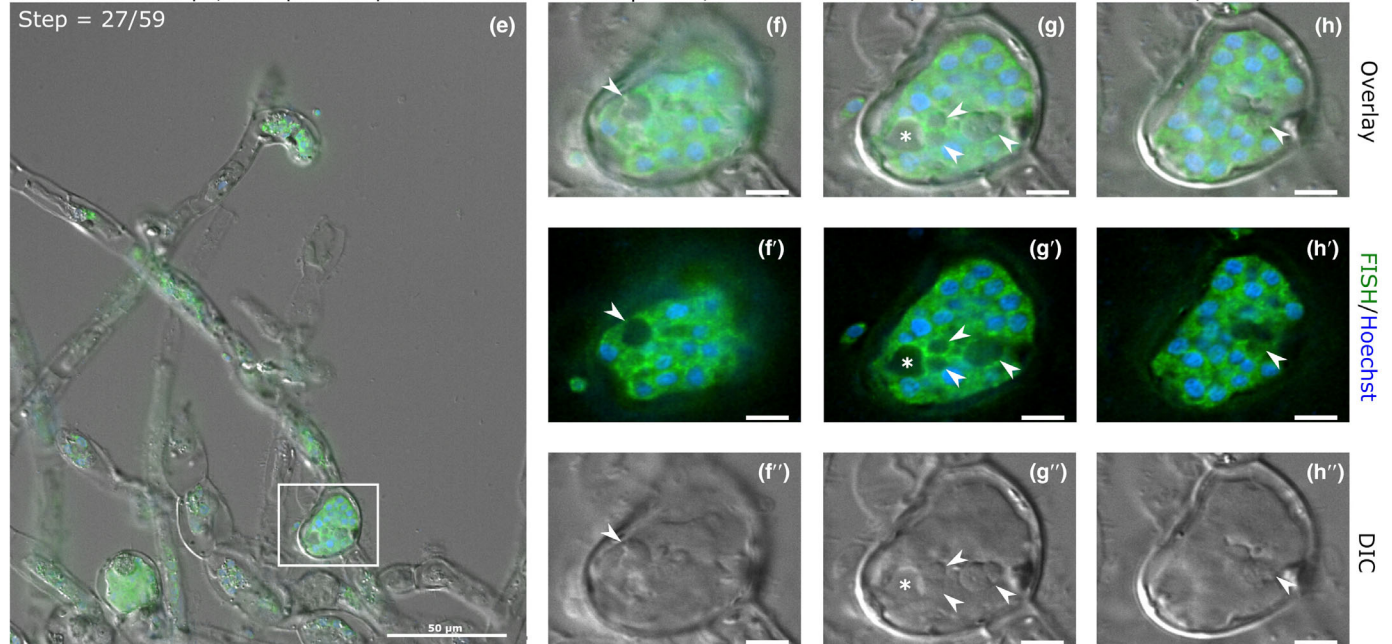
Z-stack = 63 steps, 1 step = 0.6 μm Z-stack = 59 steps, 1 step = 0.3 μm 

Fig. 2 Optical and fluorescence micrographs provide evidence of the internalization of host organelles in intracellular plasmodia of *Plasmodiophora brassicae* in *Brassica rapa* var. *pekinensis* (a–d) and of *Maullinia ectocarpii* in *Ectocarpus siliculosus* Ec32m (e–h). Images have been captured using differential interference contrast microscopy (b'–d'', f''–h'') and fluorescence microscopy (b'–d', f'–h') and subsequently overlaid (a–d, e–h). Fluorescence *in situ* hybridisation (FISH) probes specific to the 28S rRNA gene of *P. brassicae* and 18S rRNA gene of *M. ectocarpii* were used to highlight the ribosome-rich cytoplasm of the parasites (green). In fluorescence microscopy, Hoechst staining highlighted in blue the nuclei of both the parasite (small and numerous) and its host (single big nucleus in the plant host (a–d); not visible in the algal host (e–h)). White squares in (a, e) indicate the plasmodia shown in detail in (b–d) and (f–h), respectively. The white triangle in (b) points towards the Hoechst-stained host cell nucleus, while white arrowheads in (c) indicate two completely internalized starch granules. Arrowheads in (f–h) highlight engulfed algal phaeoplasts, while the asterisk in (g) indicates a vacuole. Focal planes represent a high (b, b', b'', f, f', f''), a central (c, c', c'', g, g', g'') and a low (d, d', d'', h, h', h'') layer from z-stacks containing entire plasmodia. Bars: (b–d) 10 μm ; (f–h) 5 μm .

little to no space for other structures. A second, bigger vacuole (no. 1) contains the host nucleus together with a phaeoplast, one host mitochondrion and host cytoplasm, in turn containing membranous structures interpreted as endoplasmic reticulum

and/or Golgi apparatus. An even bigger vacuole (no. 2) can be observed in Fig. 4(a,a'), within which a clearly degraded phaeoplast and two residual bodies, potentially representing a further stage in phaeoplast degradation, can be observed. The presence of

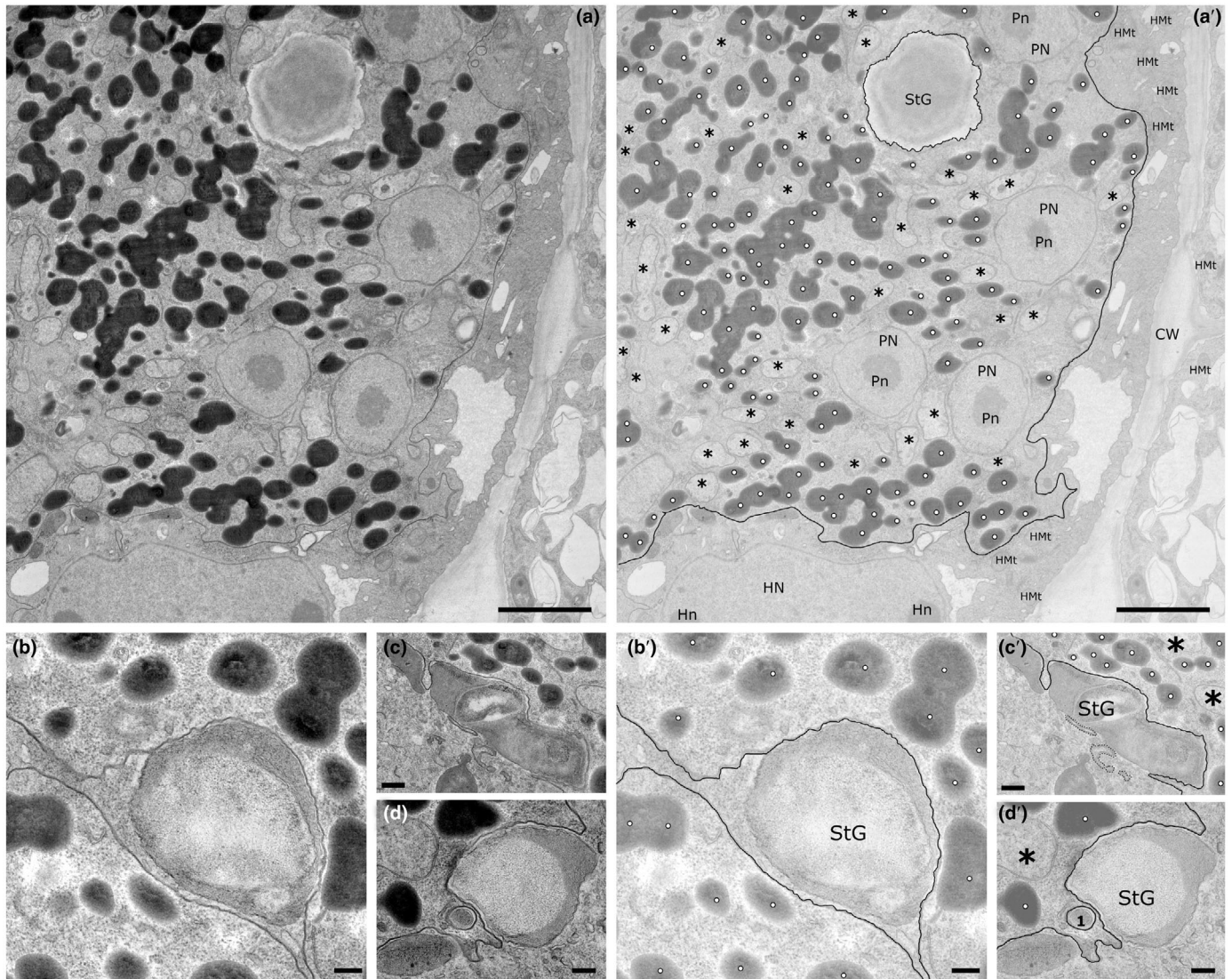


Fig. 3 Plasmodia of *Plasmodiophora brassicae* growing within the cortical cells of the root of *Brassica rapa* ssp. *pekinensis*. Annotations are provided in a separate image from the original picture (e.g. annotations for a in a', etc.). (a, a') Overview of the interface between the plasmodium and its host. Note the starch granule surrounded by the plasmodium. (b, b') Starch grain from desegregated amyloplasts is surrounded by two plasmodial protrusions, one of which is closely appressed to the granule surfaces. (c, c') Detail of plasmodial pseudopodium-like processes encircling a starch grain. (d, d') Plasma membrane invagination partially surrounding a starch grain. Note a small phagosome containing a membrane-bound, electron-opaque unidentified organelles (dashed line). In all pictures, note the presence/absence of lipid droplets and the different electron opacity/organization of the mitochondria, used as main distinctive features to tell apart host and parasite. CW, host cell wall; HMT, host mitochondria; Hn, host nucleolus; HN, host nucleus; Pn, parasite nucleolus; PN, parasite nucleus; StG, starch grains; white dots, parasite lipid droplets; *, parasite mitochondria; black lines indicate the plasma membrane of the plasmodium; solid line, plasma membrane; dotted line in (c, c'), putative plasma membrane; no. 1 in (d, d'), putative phagosome. Bars: (a, a') 2500 nm; (b, b', c, c') 500 nm; (d, d') 250 nm.

a degraded phaeoplast in vacuole 2 suggests that this has been isolated from the rest of the host cytosol and digested. Presumably, vacuoles 1 and 3 are bound to undergo the same process. The plasmodium itself is multinucleate but it has not yet undergone cytodieresis and zoospore cleavage.

Discussion

In this study, by analysing complementary lines of evidence, we demonstrate that phagocytosis is a trait that phytomyxean parasites conserved from free-living Rhizarian ancestors, adapting it

to the intracellular environment where it underpins the biotrophic interaction and where it coexists with specialized strategies of host manipulation. Molecular signatures of phagocytosis are present in all phytomyxean datasets analysed; but the model aggregates datasets in different trophic modes according to genome-based and transcriptome-based signatures (Fig. 1). These different predictions can be explained in the light of the polyphasic phytomyxean life cycle (Liu *et al.*, 2020), where the transcriptome provides a realized molecular snapshot of the feeding stage while the genome also contains genetic information on stages other than the intracellular plasmodium (e.g. free-living

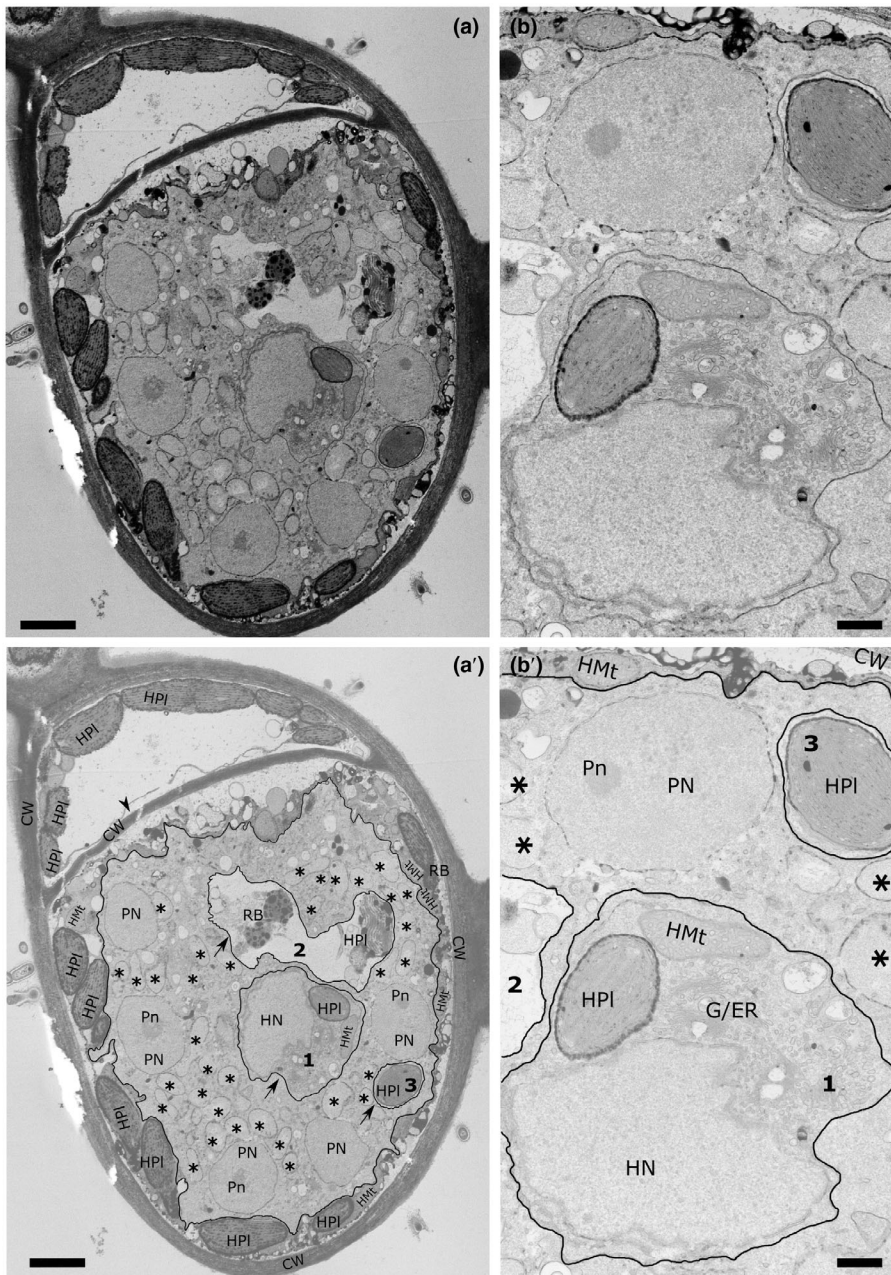


Fig. 4 Plasmodium of *Maullinia ectocarpii* growing within a cell of the gametophyte of *Macrocystis pyrifera*. Annotations are provided in a separate image from the original picture (e.g. annotations for a in a'). (a, a') Overview of the interface between the plasmodium and its host. Note the three vacuoles containing algal mitochondria, phaeoplasts and nucleus bound by membrane and surrounded by the parasite plasmodium (nos. 1–3, arrows). (b, b') Close up of (a, a') highlighting details of the algal organelles surrounded by the parasitic plasmodium. Note the difference in electron opacity/granularity between the parasite and host cytoplasm used as main distinctive features to tell apart host and parasite. Secondly, note the absence of clear tubular cristae in the putative mitochondria of *M. ectocarpii*. CW, host cell wall; HMt, host mitochondria; Hn, host nucleolus; HN, host nucleus; HPI, host phaeoplasts; Pn, parasite nucleolus; PN, parasite nucleus; RB, residual bodies; *, putative parasite mitochondria; black lines indicate the plasma membrane of the plasmodium; arrows and numbers, putative phagocytic vacuoles; arrowhead, cell wall separating infected and non-infected sectors within the same cell. Bars: (a, a') 2000 nm; (b, b') 500 nm.

flagellated zoospores). Genomic signatures identify *Phytomyxa* as phago-prototrophs while transcriptomes of intracellular parasitic stages are best explained by the subset of signatures of the intracellular phagotrophic specialist *R. allomycis* (Powell *et al.*, 2017; Fig. 1). Molecular signatures associated with the flagellum are the main drivers assigning *P. brassicae* genomes to the phago-prototrophic niche. While flagella are associated with phagotrophy in certain organisms (e.g. choanoflagellates); in *Phytomyxa*, flagella are exclusively associated with locomotion in the zoosporic phase of the life cycle but play no role in nutrition (Barr & Allan, 1982; Parodi *et al.*, 2010; Feng *et al.*, 2012). On the other hand, molecular signatures belonging to the Ras GTPases, mTORC1 and mTORC2 complexes are shared between *P. brassicae* and *M. ectocarpii* transcriptomes, both assigned to the

Rozella-like phagotrophic specialists. Ras GTPases are known to control cytoskeletal remodelling and vesicular trafficking in human phagocytes (Wiedemann *et al.*, 2005) and mTORC2 has been linked to cytoskeletal polarization related to budding in yeasts (Loewith *et al.*, 2002). Furthermore, mTOR complexes, particularly mTORC1, are known to be paramount sensors of the nutritional state of the cell acting as a switch between anabolic and catabolic metabolism; and more broadly between growth and proliferation on one hand and autophagy and apoptosis on the other (Sabatini, 2017; Condon & Sabatini, 2019). This hints at a pivotal role of perception of the nutritional state and signal transduction in the intracellular feeding plasmodia of phytomyxids, coupled with cytoskeletal rearrangements that are central for phagocytic behaviour.

interpretation, our results hint at a key role of intracellular phagocytosis in both the sporangial and sporogenic phases of the phytomyxean life cycle. *Maullinia ectocarpii* also induces mitosis and cell expansion in its algal host (Maier *et al.*, 2000) but evidence on carbohydrate accumulation in infected tissue has not yet been produced. Brown algae accumulates photosynthates mainly as soluble vacuolar laminaran and cytoplasmic mannitol (Michel *et al.*, 2010; Chabi *et al.*, 2021). It is therefore interesting to notice the early disappearance of the vacuole in cells infected by *M. ectocarpii*. Although consumption of the vacuole seems to be a necessary step of intracellular colonization, simply to provide growth space for the enlarging sporangium; this would also allow for the parasite to immediately consume the major polysaccharide storage within the host cell providing it with rapid energy. However, a first glance at levels of gene expression in *Maullinia*-infected *E. siliculosus* Ec32m did not highlight a clear pattern of upregulation of laminarin/mannitol catabolism or extra-vacuolar transport of carbohydrates (Table S2), thus whether *M. ectocarpii* manipulates its host cell carbohydrate metabolism remains unclear. It is worth reminding that the transcriptome analysed here originated from an asynchronous parasite population, where the signal of a possibly transient and/or very local interaction between the parasite and the host vacuole could have been diluted in the bulk approach used.

In the case of *M. ectocarpii*, phaeoplasts seemed to be a preferred target of phagocytosis. In fact, TEM images show that phaeoplasts in infected cells shrink with the progression of the infection (Figs 4, S4). In-depth investigation of plastidial dynamics in infected algal cells is beyond the scope of this study, but the possibility that plastids are directly manipulated before being targeted for consumption by the parasite cannot be excluded. If proven, this would hint at a conservation or convergence of the target host organelle within the Phytomyxida. Similar patterns of plastidial shrinkage have been highlighted in the interaction between the intracellular oomycete parasite *Anisolpidium ectocarpii* (infecting *M. pyrifera*), but in this case the decrease in size was interpreted as a result of autophagic processes and thus to the reaction of the host against the parasite (Murúa *et al.*, 2020).

It is worth bearing in mind that only scarce information is available on the sporogenic stage of *M. ectocarpii* (Parodi *et al.*, 2010; Blake *et al.*, 2017) and on Phagomyxida overall (Schnepf *et al.*, 2000; Murúa *et al.*, 2017). If, as it is suspected, a sporogenic phase inducing gall formation in adult kelp sporophytes does exist (Blake *et al.*, 2017), an even higher degree of host manipulation can be expected for *M. ectocarpii*, bringing it even closer to its land-dwelling relative *P. brassicae*.

Although not common, intracellular endocytosis has been documented in intracellular parasites spanning the taxa Apicomplexa (Spielmann *et al.*, 2020; and references therein), Cryptomyxota (Torruella *et al.*, 2018) and Euglenozoa (Etheridge, 2022). The reduced dataset of phagotrophy-related proteins from *R. allomycis* correctly describes *T. cruzii* and *Leishmania braziliensis* as capable of intracellular phagotrophy (Chasen *et al.*, 2020; Halliday *et al.*, 2020) while fails to assign *Plasmodium falciparum* and *T. gondii* to this category. Indeed, *P. falciparum* and *T. gondii* are known to use a different set of genes to undertake endocytic

nutrient uptake (Spielmann *et al.*, 2020) and especially to lack important genes involved in small GTPase (RAS superfamily) and TOR signalling pathways (Van Dam *et al.*, 2011), which are fundamental for the predictive model (Burns *et al.*, 2018). The apparent proximity of the genetic make-up underpinning intracellular phagocytosis in unrelated Phytomyxea, *Rozella* and trypanosomatids is intriguing, since it hints at the possibility that the smallest subset of genes required for phagocytosis is present in these otherwise unrelated parasites. Genome reduction is a well-known process in intracellular parasites (Keeling & Slamovits, 2005) and those among them which maintain a phagocytic behaviour might make a good model to investigate the very core of the phagocytic machinery, when not overly specialized towards their host or a specific substrate.

The data presented and discussed here place phytomyxean intracellular parasites half-way between the extremes of specialized biotrophic host manipulation and osmotrophy, and generalist phagocytic predation. Growing molecular and microscopic evidence suggests that phagocytosis is a backbone feature of Rhizarians upon which ‘variations on the theme’ brought about the diversification of the group (Anderson, 1978; Hirakawa, 2017; Gerbracht *et al.*, 2022; Hess & Suthaus, 2022). In this context, Phytomyxean are not an exception. It is tempting to speculate that the maintenance and adaptation of phagocytic behaviour is one of the reasons behind the success of this impactful and recalcitrant parasites, allowing them to specialize to certain hosts meanwhile maintaining the ability to feed and propagate within a broader set of organisms (Ludwig-Müller *et al.*, 1999; Maier *et al.*, 2000; Qu & Christ, 2006). Further research on this group of intriguing parasites will surely provide more evidence on the degree of host manipulation/phagocytosis within the class, especially if targeted towards non-model organisms for which data are lacking. Comparative investigations and the exploration of biodiversity surrounding parasites and pathogens prove paramount to deeply understand their biology and potentially devise strategies to counter their effects and broadly foresee the evolutionary trajectories of parasitism.

Acknowledgements

This work was funded by the Austrian Science Fund: grant Y0801-B16 (SN, MH, AG). JAB was supported in part by National Science Foundation (USA) OIA-1826734. We would like to acknowledge the assistance of Bettina Schneidhofer in the lab. Finally, the authors are thankful to all the reviewers for the insightful corrections and comments to this manuscript.

Competing interests

None declared.

Author contributions

AG and SN planned and designed the research. AG, MH, PM, WS and MK generated microscopic images and analyses. CMMG, SN, SC prepared and collected samples for molecular

analyses. AG, JAB, SC, SLH provided bioinformatics analyses and pipelines. AG and SN wrote the first draft of the manuscript which was finalized with the input of all authors.

ORCID

John A. Burns  <https://orcid.org/0000-0002-2348-8438>

Claire M. M. Gachon  <https://orcid.org/0000-0002-3702-7472>

Andrea Garvetto  <https://orcid.org/0000-0002-9525-5975>

Pedro Murúa  <https://orcid.org/0000-0002-1598-7261>

Sigrid Neuhauser  <https://orcid.org/0000-0003-0305-1615>

Data availability

Raw NGS sequences for the transcriptomic dataset of *M. ectocarpus* and its host *E. siliculosus* have been deposited in NCBI Sequence Read Archive (SRA) under the BioProject accession no. PRJNA878940. Publicly available datasets used in this work are referenced in detail by the relative publications.

References

- Abu Bakar N, Klonis N, Hanssen E, Chan C, Tilley L. 2010. Digestive-vacuole genesis and endocytic processes in the early intraerythrocytic stages of *Plasmodium falciparum*. *Journal of Cell Science* 123: 441–450.
- Aist JR, Williams PH. 1971. The cytology and kinetics of cabbage root hair penetration by *Plasmodiophora brassicae*. *Canadian Journal of Botany* 49: 2023–2034.
- Anderson OR. 1978. Light and electron microscopic observations of feeding behaviour, nutrition, and reproduction in laboratory cultures of *Thalassiosira nucleata*. *Tissue and Cell* 10: 401–412.
- Andrews S. 2010. *FASTQC: a quality control tool for high throughput sequence data*. [WWW document] URL <http://www.bioinformatics.babraham.ac.uk/projects/fastqc> [accessed 21 April 2017].
- Badstöber J, Gachon CMM, Ludwig-Müller J, Sandbichler AM, Neuhauser S. 2020. Demystifying biotrophs: FISHing for mRNAs to decipher plant and algal pathogen–host interaction at the single cell level. *Scientific Reports* 10: 14269.
- Barr DJS, Allan PME. 1982. Zoospore ultrastructure of *Polymyxa graminis* (Plasmodiophoromycetes). *Canadian Journal of Botany* 60: 2496–2504.
- Bass D, Tikhonenkov DV, Foster R, Dyal P, Janoušek J, Keeling PJ, Gardner M, Neuhauser S, Hartikainen H, Mylnikov AP *et al.* 2018. Rhizarian ‘novel clade 10’ revealed as abundant and diverse planktonic and terrestrial flagellates, including *Aquavolon* n. gen. *Journal of Eukaryotic Microbiology* 65: 828–842.
- Blake C, Thiel M, López BA, Fraser CI. 2017. Gall-forming protistan parasites infect southern bull kelp across the Southern Ocean, with prevalence increasing to the south. *Marine Ecology Progress Series* 583: 95–106.
- Bock NA, Charvet S, Burns J, Duhamel S, Kim E. 2021. Experimental identification and *in silico* prediction of bacterivory in green algae. *The ISME Journal* 15: 1987–2000.
- Bolger AM, Lohse M, Usadel B. 2014. TRIMMOMATIC: a flexible trimmer for Illumina sequence data. *Bioinformatics* 30: 2114–2120.
- Buczacki ST. 1983. *Plasmodiophora*. An inter-relationship between biological and practical problems. In: Buczacki ST, ed. *Zoospore plant pathogens. A modern perspective*. London, UK: Academic Press, 161–191.
- Bulman S, Neuhauser S. 2017. Phytomyxa. In: Archibald JM, Simpson AGB, Slamovits CH, eds. *Handbook of the protists*. Heidelberg, Germany: Springer International, 1–21.
- Burns JA, Pittis AA, Kim E. 2018. Gene-based predictive models of trophic modes suggest Asgard archaea are not phagocytotic. *Nature Ecology and Evolution* 2: 697–704.
- Cavalier-Smith T, Chao EE, Lewis R. 2018. Multigene phylogeny and cell evolution of chromist infrakingdom Rhizaria: contrasting cell organisation of sister phyla Cercozoa and Retaria. *Protoplasma* 255: 1517–1574.
- Chabi M, Leleu M, Fermont L, Colpaert M, Colleoni C, Ball SG, Cenci U. 2021. Retracing storage polysaccharide evolution in Stramenopila. *Frontiers in Plant Science* 12: 629045.
- Chasen NM, Coppens I, Etheridge RD. 2020. Identification and localization of the first known proteins of the *Trypanosoma cruzi* cytostome cytopharynx endocytic complex. *Frontiers in Cellular and Infection Microbiology* 9: 00445.
- Ciagli S, Neuhauser S, Schwelm A. 2018. Draft genome resource for the potato powdery scab pathogen *Spongospora subterranea*. *Molecular Plant–Microbe Interactions* 31: 1227–1229.
- Ciagli S, Schwelm A, Neuhauser S. 2019. Transcriptomic response in symptomless roots of clubroot infected kohlrabi (*Brassica oleracea* var. *gongyloides*) mirrors resistant plants. *BMC Plant Biology* 19: 288.
- Clay CM, Walsh JA. 1997. *Spongospora subterranea* f. sp. *nasturtii*, ultrastructure of the plasmodial-host interface, food vacuoles, flagellar apparatus and exit pores. *Mycological Research* 101: 737–744.
- Cock JM, Sterck L, Rouzé P, Scornet D, Allen AE, Amoutzias G, Anthouard V, Artiguenave F, Aury JM, Badger JH *et al.* 2010. The *Ectocarpus* genome and the independent evolution of multicellularity in brown algae. *Nature* 465: 617–621.
- Condon KJ, Sabatini DM. 2019. Nutrient regulation of mTORC1 at a glance. *Journal of Cell Science* 132: jcs222570.
- Couch JN, Leitner J, Whiffen A. 1939. A new genus of the Plasmodiophoraceae. *Journal of the Elisha Mitchell Scientific Society* 55: 399–408.
- Daval S, Belcour A, Gazengel K, Legrand L, Gouzy J, Cottret L, Lebreton L, Aigu Y, Mougel C, Manzanares-Dauleux MJ. 2018. Computational analysis of the *Plasmodiophora brassicae* genome: mitochondrial sequence description and metabolic pathway database design. *Genomics* 111: 1629–1640.
- Dou Z, MCGovern OL, Di Cristina M, Carruthers VB. 2014. *Toxoplasma gondii* ingests and digests host cytosolic proteins. *mBio* 5: 01188–14.
- Doucet M, Maia R, Eliason CM, Bitton P, Shawkey MD. 2013. PAVO: an R package for the analysis, visualization and organization of spectral data. *Methods in Ecology and Evolution* 4: 906–913.
- Dylewski DP. 1990. Phylum Plasmodiophoromycota. In: Margulis L, Corliss JO, Melkonian M, Chapman DJ, eds. *Handbook of protozoista*. Boston, MA, USA: Jones & Bartlett, 399–416.
- Dylewski DP, Miller CE, Braselton JP. 1978. Sporangial development of *Woronina pythii*. *Micron* 9: 35–36.
- Enami K, Ozawa T, Motohashi N, Nakamura M, Tanaka K, Hanaoka M. 2011. Plastid-to-nucleus retrograde signals are essential for the expression of nuclear starch biosynthesis genes during amyloplast differentiation in tobacco BY-2 cultured cells. *Plant Physiology* 157: 518–530.
- Etheridge RD. 2022. Protozoan phagotrophy from predators to parasites: an overview of the enigmatic cytostome–cytopharynx complex of *Trypanosoma cruzi*. *Journal of Eukaryotic Microbiology* 69: e12896.
- Feng J, Xiao Q, Hwang SF, Strelkov SE, Gossen BD. 2012. Infection of canola by secondary zoospores of *Plasmodiophora brassicae* produced on a nonhost. *European Journal of Plant Pathology* 132: 309–315.
- Flannagan RS, Jaumouillé V, Grinstein S. 2012. The cell biology of phagocytosis. *Annual Review of Pathology: Mechanisms of Disease* 7: 61–98.
- Gerbracht JV, Harding T, Simpson AGB, Roger AJ, Hess S. 2022. Comparative transcriptomics reveals the molecular toolkit used by an algivorous protist for cell wall perforation. *Current Biology* 32: 3374–3384.
- Godrijan J, Drapeau DT, Balch WM. 2022. Osmotrophy of dissolved organic carbon by coccolithophores in darkness. *New Phytologist* 233: 781–794.
- Grabherr MG, Haas BJ, Yassour M, Levin JZ, Thompson DA, Amit I, Adiconis X, Fan L, Raychowdhury R, Zeng Q *et al.* 2011. Full-length transcriptome assembly from RNA-Seq data without a reference genome. *Nature Biotechnology* 29: 644–652.
- Halliday C, De Castro-neto A, Alcántara CL, Cunha-e-silva NL, Vaughan S, Sunter JD. 2020. Trypanosomatid flagellar pocket from structure to function. *Trends in Parasitology* 37: 317–329.
- Held A. 1975. The zoospore of *Rozella allomycis*: ultrastructure. *Canadian Journal of Botany* 1: 2212–2232.

- Hess S, Suthaus A. 2022. The Vampyrellid amoeba (Vampyrellida, Rhizaria). *Protist* 173: 125854.
- Hirakawa Y. 2017. Chlorarachniophytes with complex secondary plastids of green algal origin. In: Hirakawa Y, Jacquot J-P, Gadal P, eds. *Advances in botanical research*, vol. 84. Oxford, UK: Oxford Academic Press, 359–394.
- Hittorf M, Letsch-praxmarer S, Windegger A, Bass D, Kirchmaier M, Neuhauser S. 2020. Revised taxonomy and expanded biodiversity of the Phytomyxea (Rhizaria, Endomyxa). *Journal of Eukaryotic Microbiology* 67: 648–659.
- Hossain M, Pérez-lópez E, Todd CD, Wei Y, Bonham-smith PC. 2021. Endomembrane-targeting *Plasmodiophora brassicae* effectors modulate PAMP triggered immune responses in plants. *Frontiers in Microbiology* 12: 651279.
- James TY, Pelin A, Bonen L, Ahrendt S, Sain D, Corradi N, Stajich JE. 2013. Shared signatures of parasitism and phylogenomics unite cryptomycota and microsporidia. *Current Biology* 23: 1548–1553.
- Jimenez V, Burns JA, Le Gall F, Not F, Vault D. 2021. No evidence of phagomixotrophy in *Micromonas polaris* (Mamiellophyceae), the dominant picophytoplankton species in the Arctic. *Journal of Phycology* 57: 435–446.
- Jones P, Binns D, Chang HY, Fraser M, Li W, McAnulla C, McWilliam H, Maslen J, Mitchell A, Nuka G *et al.* 2014. INTERPROSCAN 5: genome-scale protein function classification. *Bioinformatics* 30: 1236–1240.
- Kamennaya NA, Kennaway G, Fuchs BM, Zubkov MV. 2018. “Pomacytosis” – semi-extracellular phagocytosis of cyanobacteria by the smallest marine algae. *PLoS Biology* 16: e2003502.
- Karling J. 1944. *Phagomyxa algarum* n. gen., n. sp., an unusual parasite with plasmodiophoralean and proteomyxean characteristics. *American Journal of Botany* 31: 38–52.
- Keeling PJ. 2019. Combining morphology, behaviour and genomics to understand the evolution and ecology of microbial eukaryotes. *Philosophical Transactions of the Royal Society of London. Series B: Biological Sciences* 374: 20190085.
- Keeling PJ, Slamovits CH. 2005. Causes and effects of nuclear genome reduction. *Current Opinion in Genetics and Development* 15: 601–608.
- Keskin B, Fuchs WH. 1969. Der infektionsvorgang bei *Polymyxa betae*. *Archiv für Mikrobiologie* 68: 218–226.
- Keymer A, Pimprikar P, Wewer V, Huber C, Brands M, Bucarius SL, Delaux P, Klingl V, Wang TL, Eisenreich W. 2017. Lipid transfer from plants to arbuscular mycorrhizal fungi. *eLife* 6: e29107.
- Kolátková V, Čepička I, Hoffman R, Vohník M. 2020. *Marinomyxa* gen. nov. accommodates gall-forming parasites of the tropical to subtropical seagrass genus *Halophila* and constitutes a novel deep-branching lineage within Phytomyxea (Rhizaria: Endomyxa). *Microbial Ecology* 81: 673–686.
- Kong L, Li X, Zhan Z, Piao Z. 2022. Sugar transporters in *Plasmodiophora brassicae*: genome-wide identification and functional verification. *International Journal of Molecular Sciences* 23: 5264.
- Langmead B, Salzberg SL. 2012. Fast gapped-read alignment with BOWTIE 2. *Nature Methods* 9: 357–359.
- Li B, Dewey CN. 2011. RSEM: accurate transcript quantification from RNA-Seq data with or without a reference genome. *BMC Bioinformatics* 12: 323.
- Liu J, Williams TA, Burns JA. 2021. Relating genome completeness to functional predictions. *bioRxiv*. doi: 10.1101/2021.10.01.462806.
- Liu L, Qin L, Zhou Z, Hendriks WGHM, Liu S, Wei Y. 2020. Refining the life cycle of *Plasmodiophora brassicae*. *Phytopathology* 110: 1704–1712.
- Loewith R, Jacinto E, Wullschlegel S, Lorberg A, Oppliger W, Jenoe P, Hall MN. 2002. Two TOR complexes, only one of which is rapamycin sensitive, have distinct roles in cell growth control. *Molecular Cell* 10: 457–468.
- Ludwig-Müller J, Bennett RN, Kiddle G, Ihmig S, Ruppel M, Hilgenberg W. 1999. The host range of *Plasmodiophora brassicae* and its relationship to endogenous glucosinolate content. *New Phytologist* 141: 443–458.
- Ma Y, Choi SR, Wang Y, Chhakekar SS, Zhang X, Wang Y, Zhang X, Zhu M, Liu D, Zuo Z *et al.* 2022. Starch content changes and metabolism-related gene regulation of Chinese cabbage synergistically induced by *Plasmodiophora brassicae* infection. *Horticulture Research* 9: uhab071.
- Maier I, Parodi E, Westermeier R, Müller DG. 2000. *Maullinia ectocarpii* gen. et sp. nov. (Plasmodiophorea), an intracellular parasite in *Ectocarpus siliculosus* (Ectocarpales, Phaeophyceae) and other filamentous brown algae. *Protist* 151: 225–238.
- Malinowski R, Truman W, Blicharz S. 2019. Genius architect or clever thief – how *Plasmodiophora brassicae* reprograms host development to establish a pathogen-oriented physiological sink. *Molecular Plant–Microbe Interactions* 32: 1259–1266.
- Matz JM, Beck JR, Blackman MJ. 2020. The parasitophorous vacuole of the blood-stage malaria parasite. *Nature Reviews Microbiology* 18: 379–391.
- Michel G, Tonon T, Scornet D, Cock JM, Kloareg B. 2010. Central and storage carbon metabolism of the brown alga *Ectocarpus siliculosus*: insights into the origin and evolution of storage carbohydrates in Eukaryotes. *New Phytologist* 188: 67–81.
- Miura T, Moriya H, Iwai S. 2017. Assessing phagotrophy in the mixotrophic ciliate *Paramecium bursaria* using GFP-expressing yeast cells. *FEMS Microbiology Letters* 364: fnx117.
- Moreira D, Lopez-Garcia P. 2014. The rise and fall of Picobiliphytes: how assumed autotrophs turned out to be heterotrophs. *BioEssays* 36: 468–474.
- Murúa P, Goetze F, Westermeier R, van West P, Küpper FC, Neuhauser S. 2017. *Maullinia braseltonii* sp. nov. (Rhizaria, Phytomyxea, Phagomyxida): a cyst-forming parasite of the bull kelp *Durvillaea* spp. (Stramenopila, Phaeophyceae, Fucales). *Protist* 168: 468–480.
- Murúa P, Müller DG, Etemadi M, van West P, Gachon CMM. 2020. Host and pathogen autophagy are central to the inducible local defences and systemic response of the giant kelp *Macrocystis pyrifera* against the oomycete pathogen *Anisopidium ectocarpii*. *New Phytologist* 226: 1445–1460.
- Not F, De Roscoff SB, Valentin K, Lovejoy C. 2007. Picobiliphytes: a marine picoplanktonic algal group with unknown affinities to other eukaryotes. *Science* 315: 253–255.
- Olszak M, Truman W, Stefanowicz K, Sliwinski E, Ito M, Walerowski P, Rolfé S, Malinowski R. 2019. Transcriptional profiling identifies critical steps of cell cycle reprogramming necessary for *Plasmodiophora brassicae*-driven gall formation in *Arabidopsis*. *The Plant Journal* 97: 715–729.
- Parodi ER, Cáceres EJ, Westermeier R, Müller DG. 2010. Secondary zoospores in the algal endoparasite *Maullinia ectocarpii* (Plasmodiophoromycota). *Biocell* 34: 45–52.
- Pendergrass WR. 1950. Studies on a Plasmodiophoraceous parasite, *Octomyxa brevilegniae*. *Mycologia* 42: 279–289.
- Pérez-López E, Hossain MM, Tu J, Waldner M, Todd CD, Kusalik AJ, Wei Y, Bonham-Smith PC. 2020. Transcriptome analysis identifies *Plasmodiophora brassicae* secondary infection effector candidates. *Journal of Eukaryotic Microbiology* 67: 337–351.
- Pérez-López E, Hossain MM, Wei Y, Todd CD, Bonham-smith PC. 2021. A clubroot pathogen effector targets cruciferous cysteine proteases to suppress plant immunity. *Virulence* 12: 2327–2340.
- Powell MJ, Letcher PM, James TY. 2017. Ultrastructural characterization of the host–parasite interface between *Allomyces anomalus* (Blastocladiomycota) and *Rozella allomycis* (Cryptomycota). *Fungal Biology* 121: 561–572.
- Qu X, Christ BJ. 2006. The host range of *Spongopora subterranea* f. sp. *subterranea* in the United States. *American Journal of Potato Research* 83: 343–347.
- Raven JA, Beardall J, Flynn KJ, Maberly SC. 2009. Phagotrophy in the origins of photosynthesis in eukaryotes and as a complementary mode of nutrition in phototrophs: relation to Darwin’s insectivorous plants. *Journal of Experimental Botany* 60: 3975–3987.
- Rolfé SA, Strelkov SE, Links MG, Clarke WE, Robinson SJ, Djavaheri M, Malinowski R, Haddadi P, Kagale S, Parkin IAP *et al.* 2016. The compact genome of the plant pathogen *Plasmodiophora brassicae* is adapted to intracellular interactions with host *Brassica* spp. *BMC Genomics* 17: 272.
- Sabatini DM. 2017. Twenty-five years of mTOR: uncovering the link from nutrients to growth. *Proceedings of the National Academy of Sciences, USA* 114: 11818–11825.
- Schmieder R, Edwards R. 2011. Fast identification and removal of sequence contamination from genomic and metagenomic datasets. *PLoS ONE* 6: e17288.
- Schnepf E. 1994. A *Phagomyxa*-like endoparasite of the centric marine diatom *Bellerophonella malleus*: a phagotrophic plasmodiophoromycete. *Botanica Acta* 107: 374–382.

- Schnepf E, Kühn SF, Bulman S. 2000. *Phagomyxa bellerocbeae* sp. nov. and *Phagomyxa odontellae* sp. nov., plasmodiophoromycetes feeding on marine diatoms. *Helgoland Marine Research* 54: 237–242.
- Schwelm A, Berney C, Dixelius C, Bass D, Neuhauser S. 2016. The large subunit rDNA sequence of *Plasmodiophora brassicae* does not contain intra-species polymorphism. *Protist* 167: 544–554.
- Schwelm A, Fogelqvist J, Knaust A, Jülke S, Lilja T, Bonilla-Rosso G, Karlsson M, Shevchenko A, Dhandapani V, Choi SR *et al.* 2015. The *Plasmodiophora brassicae* genome reveals insights in its life cycle and ancestry of chitin synthases. *Scientific Reports* 5: 11153.
- Seenivasan R, Sausen N, Medlin LK, Melkonian M. 2013. *Picomonas judraskeda* gen. et sp. nov.: the first identified member of the Picozoa phylum nov., a widespread group of picoeukaryotes, formerly known as “picobiliophytes”. *PLoS ONE* 8: e59565.
- Sierra R, Canas-Duarte SJ, Burki F, Schwelm A, Fogelqvist J, Dixelius C, González-García LN, Gile GH, Slamovits CH, Klopp C *et al.* 2016. Evolutionary origins of rhizarian parasites. *Molecular Biology and Evolution* 33: 980–983.
- Simão FA, Waterhouse RM, Ioannidis P, Kriventseva EV, Zdobnov EM. 2015. BUSCO: assessing genome assembly and annotation completeness with single-copy orthologs. *Bioinformatics* 31: 3210–3212.
- Spielmann T, Gras S, Sabitzki R, Meissner M. 2020. Endocytosis in *Plasmodium* and *Toxoplasma* parasites. *Trends in Parasitology* 36: 520–532.
- Stjelja S, Fogelqvist J, Tellgren-Roth C, Dixelius C. 2019. The architecture of the *Plasmodiophora brassicae* nuclear and mitochondrial genomes. *Scientific Reports* 9: 15753.
- Talley MR, Miller CE, Braselton JP. 1978. Notes on the ultrastructure of zoospores of *Sorosphaera veronicae*. *Mycologia* 70: 1241–1247.
- Tanaka S, Ito SI, Kameya-Iwaki M. 2001. Electron microscopy of primary zoosporogenesis in *Plasmodiophora brassicae*. *Mycoscience* 42: 389–394.
- Torruella G, Grau-Bové X, Moreira D, Karpov SA, Sebé-pedros A, Völcker E, López-garcía P, Burns JA. 2018. Global transcriptome analysis of the aphelid *Paraphelidium tribonemae* supports the phagotrophic origin of fungi. *Nature Communications* 1: 231.
- Uribe-Querol E, Rosales C. 2020. Phagocytosis: our current understanding of a universal biological process. *Frontiers in Immunology* 11: 01066.
- Van Dam TJP, Zwartkruis FJT, Bos JL, Snel B. 2011. Evolution of the TOR pathway. *Journal of Molecular Evolution* 73: 209–220.
- Voleman L, Doležal P. 2019. Mitochondrial dynamics in parasitic protists. *PLoS Pathogens* 15: 1–15.
- Wiedemann A, Lim J, Caron E. 2005. Small GTP binding proteins and the control of phagocytic uptake. In: Rosales C, ed. *Molecular mechanisms of phagocytosis*. New York, NY, USA: Springer, 72–84.
- Williams PH, McNabola SS. 1967. Fine structure of *Plasmodiophora brassicae* in sporogenesis. *Canadian Journal of Botany* 45: 1665–1669.
- Williams PH, McNabola SS. 1970. Fine structure of the host-parasite interface of *Plasmodiophora brassicae*. *Phytopathology* 60: 1557–1561.
- Yutin N, Wolf MY, Wolf YI, Koonin EV. 2009. The origins of phagocytosis and eukaryogenesis. *Biology Direct* 4: 9.

Supporting Information

Additional Supporting Information may be found online in the Supporting Information section at the end of the article.

Fig. S1 BUSCO analysis of the genomes and transcriptomes of all Phytomyxid analysed.

Fig. S2 Optical and fluorescence micrographs provide evidence of phagocytosis in intracellular plasmodia of *Maullinia ectocarpii* in *Macrocystis pyrifera*.

Fig. S3 Young plasmodium of *Maullinia ectocarpii* in its host alga *Macrocystis pyrifera*.

Fig. S4 Comparison of TEM images of mitochondria of different phytomyxea and life cycle stages.

Fig. S5 Changes in *Brassica oleracea* starch metabolism during infection from *Plasmodiophora brassicae*.

Notes S1 Comparison between best-hit genes against molecular signatures of general phagotrophy.

Notes S2 Accompanying video for Fig. 2.

Notes S3 Accompanying video for Fig. S2.

Table S1 Values from the TROPICMODEPREDICTIONTOOL assigning the proteomes of the listed organisms to five different trophic modes.

Table S2 Log₂ fold change expression levels in *Maullinia*-infected *Ectocarpus siliculosus* Ec32m vs non-infected control for enzymes involved in carbohydrate metabolism.

Please note: Wiley is not responsible for the content or functionality of any Supporting Information supplied by the authors. Any queries (other than missing material) should be directed to the *New Phytologist* Central Office.